THEORY VERSUS EXPERIMENT OF THE ROTORDYNAMIC AND LEAKAGE CHARACTERISTICS OF SMOOTH ANNULAR BUSHING OIL SEALS

A Thesis

by

VITTORIO GIUSEPPE CULOTTA

Submitted to the Office of Graduate Studies of
Texas A&M University
in partial fulfillment of the requirements for the degree of

MASTER OF SCIENCE

December 2004

Major Subject: Mechanical Engineering

THEORY VERSUS EXPERIMENT OF THE ROTORDYNAMIC AND LEAKAGE CHARACTERISTICS OF SMOOTH ANNULAR BUSHING OIL SEALS

A Thesis

by

VITTORIO GIUSEPPE CULOTTA

Submitted to Texas A&M University
in partial fulfillment of the requirements
for the degree of

MASTER OF SCIENCE

Approved as to style and content by:

Dara W. Childs (Chair of Committee)	John M. Vance (Member)
Charles Harris (Member)	

Dennis L. O'Neal
(Head of Department)

December 2004

Major Subject: Mechanical Engineering

ABSTRACT

Theory versus Experiment of the Rotordynamic and Leakage Characteristics of Smooth Annular Bushing Oil Seals. (December 2004)
Vittorio Giuseppe Culotta, B.S., Louisiana Tech University
Chair of Advisory Committee: Dr. Dara W. Childs

This thesis provides a comparison of experimental rotordynamic coefficients for laminar, smooth bushing oil seals to theoretical predictions from XLLubeGT and XLAnSeal. The experimental results come from a new test rig developed at the Turbomachinery Laboratory at Texas A&M University. The two software programs were developed to predict the static and dynamic characteristics of seals. XLLubeGT is a Reynolds equation based program while XLAnSeal is based on a bulk-flow Navier-Stokes model that includes temporal and convective acceleration terms. XLAnSeal was used to predict the added-mass terms of the seals since XLLubeGT assumes those terms to be zero or negligible. The data used for input into the two seals code was the actual measured conditions from the test rig. As part of the input parameters, inlet inertia effects and thermal gradients along the seal were included. Both XLLubeGT and XLAnSeal have the capability to analyze straight bore seals with different inlet and outlet clearances – essentially a tapered seal – but seal expansion caused by the radial differential pressure across the seal bushing was not included.

Theoretical and experimentally determined dynamic characteristics include stiffness, damping, inertia terms and Whirl Frequency Ratio (WFR). Seal static characteristics are also reported. They include: leakage, shaft center line loci and Reynolds numbers. Test conditions include three shaft speeds: 4000, 7000 and 10,000 rpm, three test pressures: 21, 45 and 69 bar [300, 650, and 1000 psi] and multiple eccentricities from 0.0 to 0.7. The results for the dynamic characteristics show good correlation of the experimental data to the theoretical values up to an eccentricity of about 0.5. At higher eccentricities, the theory generally under-predicts the dynamic

characteristics. Inertia terms are greatly under-predicted. The results for the static characteristics also show good correlation to the experimental data, but they also have a tendency to be under-predicted at higher eccentricities.

DEDICATION

I would like to dedicate this paper and entire scope of work to all of those people who continually seek the light of truth and seek to expand their minds through the exercise of thought and reason. May their triumphs and failures lead them to great discoveries both big and small.

ACKNOWLEDGEMENTS

I would like to thank everyone. No, really. There have been so many people who have helped me along the way from the time I began this little adventure over 6 years ago. I would like to thank all of my fellow graduate research assistants for providing companionship, a different perspective on the world and help on homework. I would like to thank all of the student workers whose time and talent have helped this project move along. I thank Dr. Childs, Dr. Vance and Dr. Harris for being patient with me when I was slow to understand and for guiding me along this path of higher education.

But most of all I would like to thank my wonderful family for all of the sacrifices they made so that I could finish this work. I would especially like to thank my beautiful wife for her extraordinary sacrifices. I would like to thank her for all the diapers she changed, all of the dishes she washed, all of the laundry she did, all of the baths she gave our kids just so I could finish this paper - even though it was my turn to do them. You are more than amazing, you are the best wife, friend and mother to his children a person could ask for. I love you. Let's party.

NOMENCLATURE

$\boldsymbol{A_{ij}}$	Fourier transforms for the measured stator acceleration. (e.g. A_{ij} is the acceleration in "j" direction, due to an excitation force in the "i" direction) [L/t^2]
C_{ij}	Direct and cross-coupled damping coefficients [F-t/L]
C_r	Radial seal clearance [L]
D	Seal Inner diameter [L]
$\boldsymbol{D_{ij}}$	Fourier transforms for the measured stator relative motion [L]
e_x e_y	Seal equilibrium position in the *x* and *y* directions [L]
$\boldsymbol{F_{ij}}$	Fourier transforms for the measured stator force [F]
F_s	Static force applied by pneumatic loader [F]
f_{sx} f_{sy}	Seal reaction force component in the *x,y* direction respectively [F]
f_x f_y	Measured excitation force component in the *x,y* direction [F]
F_{Seal_X} F_{Seal_y}	Calculated excitation force component in the *x,y* direction [F]
$\boldsymbol{H_{ij}}$	Direct and cross-coupled dynamic stiffness [F/L]
$\boldsymbol{J}$	Imaginary unit, $\sqrt{-1}$ [-]
K_{ij}	Direct and cross-coupled stiffness coefficients [F/L]
L	Seal length [L]
M_s	Mass of the stator [M]
M_{ij}	Direct and cross-coupled added-mass coefficients [M]
$\dot{Q}$	Seal oil supply flow rate [L^3/t]
r	Seal radius [L]
Re_{Circ}	Reynolds number, Circumferential, $\frac{\rho \cdot \omega \cdot r \cdot Cr}{\mu}$ [-]
Re_{Axial}	Reynolds number, Axial, $\rho \frac{\dot{Q}}{2\pi r \mu}$ [-]

$Re_{Squeeze}$	Reynolds number, Squeeze, $\frac{\rho \cdot \omega \cdot Cr^2}{\mu}$ [-]
T_{in}	Oil inlet temperature [T]
T_{out}	Oil outlet temperature (average of the Non-Driven and Driven-End temperatures) [T]
$\ddot{x}_s \ \ddot{y}_s$	Absolute acceleration of the stator in the *x,y* direction [L/t^2]
$\Delta x \ \Delta y$	Relative motion between the rotor and the stator in the *x,y* directions [L]
ε	Eccentricity ratio [-]
Λ	Square of the excitation frequency, Ω^2 [(1/t)^2]
ρ	Lubricant density [M/L^3]
ω	Running speed of rotor [1/t]
Ω	Excitation frequency of stator [1/t]
μ	Lubricant viscosity of test seal oil in Pa-sec [M/L-t]

Subscripts

x,y	*x* and *y* direction (defined in Fig. 9)
i,j	*x,y*

Abbreviations

RPM	Revolutions per minute
DE, NDE	Driven End, Non-Driven End

TABLE OF CONTENTS

Page

LIST OF FIGURES

Page

LIST OF TABLES

Page

INTRODUCTION

All of today's high-speed rotating machinery or "turbomachinery", whether pumps, centrifugal compressors or turbines, require an important piece of equipment: seals. Annular seals are non-contacting, non-rotating elements that are used to separate two regions of different pressure and reduce leakage across the boundaries of those regions. "Non-contacting" is defined as when there is clearance between the rotating shaft OD and the non-rotating seal ID. These two regions may be the internal process pressures and the atmosphere (such as an open drain system) or they may be a high pressure and a low pressure stage within the machine.

Figure 1 shows a detailed cross section of a single break-down high pressure oil seal cartridge. The seal cartridge contains two elements loaded by a series of springs to assist in initial assembly and pressurization of the seals.

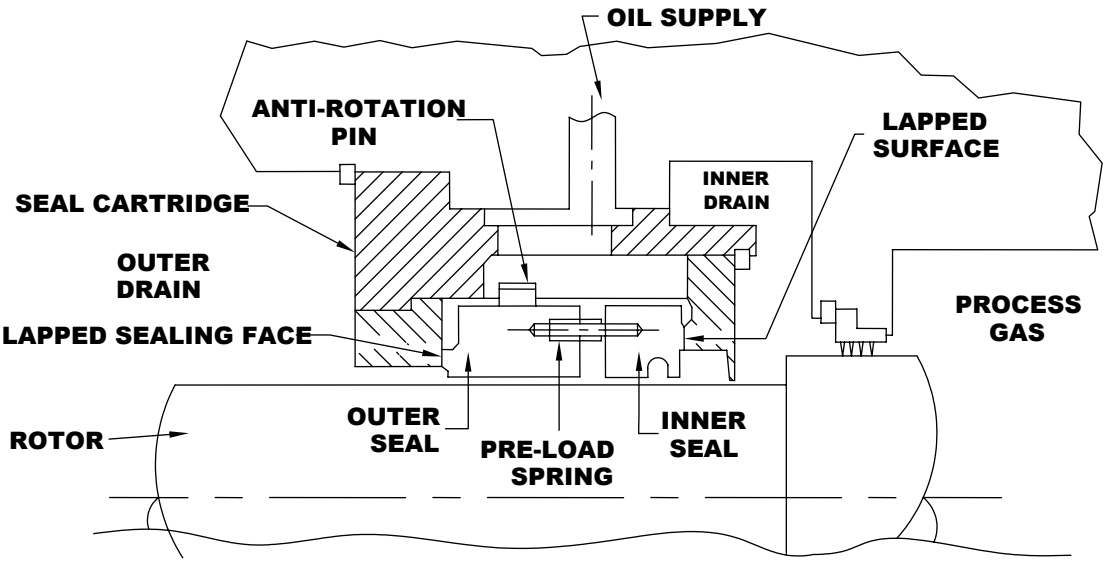

Fig. 1 - Cross section of a single break-down high pressure oil seal cartridge [1]

This thesis follows the style and format of the ASME Journal of Tribology.

The process gas is at the suction pressure, P_s, while oil is supplied at pressure $P_s + \Delta P$. The seal segments consist of outer and inner seals which are spring-loaded against each other. The preload of the spring causes the lapped external faces of the seal segments to be in contact with the seal cartridge housing. An anti-rotation pin is provided to prevent rotation of the seal segments, but it will allow the seal to move radially or "float". Oil enters the seal cartridge between the two seal segments and then leaks axially along the rotating shaft. Most of the oil is recovered. However, a portion is generally lost to the process gas stream.

Floating oil seals are of interest in the rotordynamic analysis of compressors because the fluid annuli act as plain journal bearings once they "lock-up". Floating oil seals will lock-up when the pressure-drop across the seal creates a friction force on the sealing faces (Fig. 1) greater than the circumferential fluid forces caused by the rotating shaft on the floating seal ring. Locked-up seals tend to have direct stiffness and direct damping which aid in the stability of the system, but they also tend to have much larger values for cross-coupled stiffness which tends to degrade the system stability. The conventional physical representation of the coefficients that are of interest in this work are shown in figure 2. Note the figure does not include any added mass terms (M) which this paper will show are significant in value. Rotordynamic coefficients for plain seals generally show only minor dependence on running speed and differential pressure; rather they are heavily dependent on the rotor eccentricity which leads back to the problem of seal lock-up. Note also that seal leakage rates are dependent upon the differential pressure – i.e. leakage increases with pressure. Once a seal has locked-up, it can create rotordynamic instabilities for the rotor ("self-excited whirl") caused by a reaction force ("follower force") in the direction of rotation. This reaction force is created when the cross-coupled stiffnesses have opposite signs and the available damping is not sufficient enough to attenuate this "follower force".[2]

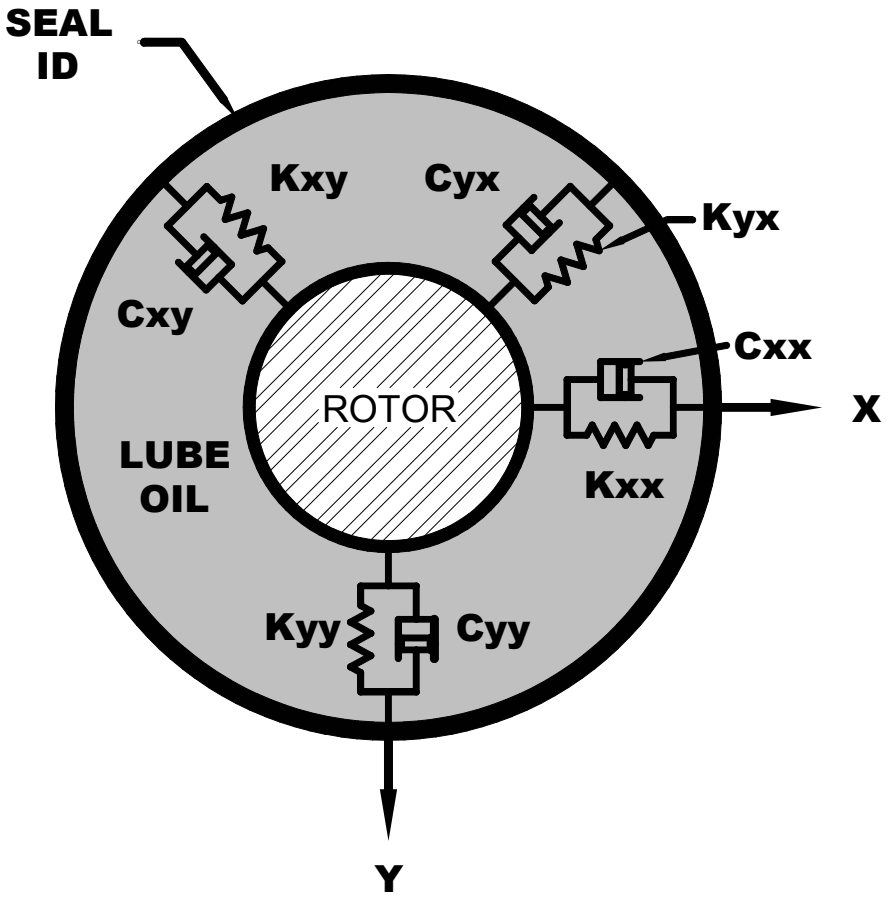

Fig. 2 - Conventional physical interpretation of linearized seal coefficients

The experimental results presented in this thesis are compared to predictions from the XLLubeGT[1] and XLAnSeal computer codes[2]. XLAnSeal was selected because it has the capability to predict the added-mass terms of seals. The experimental results come from a new test rig developed at the Turbomachinery Laboratory at Texas A&M University.

---

[1] Developed by Semantes and San Andres [3] of the Texas A&M Turbomachinery Laboratory.

[2] Both programs are part of the XLTRC© Rotordynamics Software Suite that was created at the Texas A&M Turbomachinery Laboratory.

The test seal is a smooth bore annular seal manufactured from 660 Bronze. The nominal ID is 116 mm [4.6 in] and nominal length is 24.9 mm [0.98 in] (Length-to-diameter ratio is 0.21 - “short seal”). The seal radial clearance is 0.085 mm [0.0033 in]. Test conditions include three shaft speeds: 4000, 7000 and 10,000 rpm, three test pressures: 21, 45 and 69 bar [300, 650, and 1000 psi] and multiple eccentricities from 0.0 to 0.7.

LITERATURE REVIEW

Even though oil seals have been used widely in industry for many years, no one had carried out a significant analysis of the dynamic characteristics of laminar flow oil seals until 1979 when Kirk and Miller [1] published an analysis for their characteristics using Ockvirk's short-bearing solution to the Reynolds equation. With data gathered from field tests on full scale compressors, Kirk and Miller concluded that, "this type of analysis was sufficient for design studies and modifications to enhance the response and stability of turbo-compressors using ring seals". There was some previous work done by Black and Jenssen [4] and Black and Cochrane [5] in regards to the analysis of turbulent annular pump seals using a bulk-flow Navier-Stokes model. But these analyses were for high differential pressure, small clearance water seals. These seals are characterized by high axial Reynolds numbers ($Re > 2000$). Oil seals tend to be characterized by lower axial Reynolds numbers; therefore, a laminar-flow Reynolds equation model is more appropriate. Kirk and Nichols [6] expanded Kirk and Miller's [1] previous analysis to include a heat balance to account for the heat created by hydrodynamic and fluid extrusion effects. Their analysis showed significant temperature increases along the length of the seal. Reedy and Kirk [7] continued to expand this analysis by including pressure and temperature dependent viscosities. Reedy and Kirk concluded that temperature gradients needed to be included in order to obtain the correct pressure distribution from which the dynamic characteristics are determined. For example, their results show a 17% difference in the cross-coupled stiffness terms that were calculated with an average seal temperature versus those calculated with a linear temperature gradient.

In 1996, Venkatarman and Palazzolo [8] showed that the pressure differential across the seal bore could actually deflect the seal, effectively turning a straight bore annular seal into a convergent taper seal. They also concluded that these deflections could have significant effects on the rotordynamic coefficients of a seal. Their work actually covered turbulent cryogenic annular seals used in the Space Shuttle Main

Oxygen Turbo Pumps operating up to 20 MPa, but their results are valid for seals operating at lower differential pressures that are great enough to deflect the seal and seal housing. Bahetti and Kirk [9], performed a ThermoHydroDynamic analysis on oil seals with and without the mechanical expansion caused by the radial pressure distribution across the seal bushing. They concluded that including these deflections could actually be advantageous because the analysis that did not include them under-predicted the direct stiffness and damping as well as the cross-coupled stiffness. The leakage was also over-predicted.

A number of articles, including those by Kirk and Miller [1] and Tanaka [10], report on field results for rotating equipment with instability problems caused by annular seals and how they were fixed. In 1986, Kirk, McKenna and Kraft [11] outlined an experimental program to determine the dynamic characteristics of ring seals; however, no results for rotordynamic coefficients were provided. Kirk and Browne [12] reported on their results from a non-rotating, low pressure 6.89 bars (max) [100 psi] test rig that determined the holding forces in floating ring seals. Their analysis also showed that the pitch of the rotor should not be ignored in determining the dynamic forces produced from oil seals.

Kaneko [13] presented some of the first experimentally determined static and dynamic coefficients for plain oil seals. His analysis compared the results to laminar and turbulent Reynolds equations which were solved numerically. The pressure drop due to axial acceleration of the liquid at the inlet of the seal was also included. His theory and experimental data showed good agreement. The only issues with Kankeo's results is that they were done at relatively low speed – 4000 RPM max and relatively low pressures – 1.5 bars (227 psi) max. He also does not mention what excitation frequencies where used (can not determine if coefficients are frequency dependent), and the shaft OD was relatively small - 2.75" (therefore low surface speeds). Essentially, the tests were not "real world" conditions.

DESCRIPTION OF THE TEST RIG [3]

OVERVIEW

Figure 3 depicts the test rig used to measure the static and dynamic performance of annular oil seals. Kaul [14] presents a detailed account of the design and features of the test rig and facility at the Texas A&M Turbomachinery Laboratory. A summary of its main features follows.

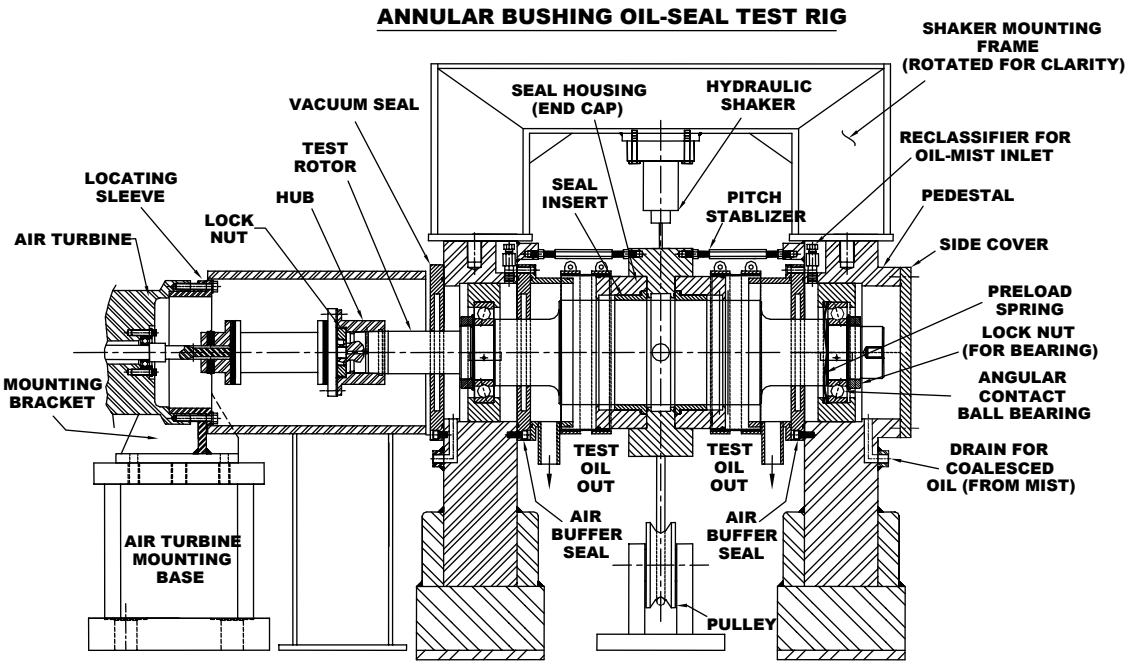

Fig. 3 - Test rig section view

The rig consists of a steel base that supports the main test section and the air turbine that drives the shaft. The shaft is connected to a 33.5 kW-power [45 hp] air turbine with a high-speed flexible disc coupling and can run up to a maximum speed of

[3] This section is adapted with permission from Rodriguez [2]

17,000 rpm. The test shaft is made from stainless steel and machined to a precise diameter of 116.84 mm [4.6 in] at the test section. It is supported on the pedestals through angular contact ball bearings, spaced approximately 430 mm [16.9 in] apart. An oil-mist lubrication system is used for lubricating the ball bearings.

A stator section holds the test seals and all the associated instrumentation, namely, non-contacting eddy-current proximity sensors, accelerometers, pressure transducers and thermocouples. A pneumatic loader and two hydraulic shakers apply static and dynamic loads to the stator. Angular alignment between the seals and the shaft is adjusted via an arrangement of six pitch stabilizers.

ISO VG32 turbine oil is delivered to the test section from an oil supply system. The oil supply system can deliver oil up to a maximum pressure of 82.7 bars [1200 psi] and a volumetric flow of 75 liters per minute [19.8 GPM]. A heat exchanger and a set of pneumatically driven valves allow for control of the temperature of the oil being delivered to the test section.

LOADING CONFIGURATION

Two orthogonally mounted hydraulic shaker heads are attached to the stator middle section. The shaker-stinger-stator arrangement is shown in Fig. 4, as observed from the non-driven end. The shaker in the x-direction can excite the stator with dynamic loads up to 4450 N [1000 lbf] in tension and compression; the shaker in the y-direction can excite the stator with dynamic loads up to 4450 N in tension and 11,125 N [2500 lbf] in compression. Both shakers can provide excitation frequencies up to 1000 Hz.

The shaker heads are attached to the stators through beam elements called stingers. Stingers isolate the test structure from the dynamics of the shaker's structure. The load applied to the stator is measured via load cells mounted inline with the shaker heads and stingers.

While the shakers provide dynamic loads exclusively, the pneumatic loader applies a static tensile load to the stator in one direction. Fig. 5 shows the static loader assembly. The stator is displaced in the $+y$ direction due to the static load. A cable is

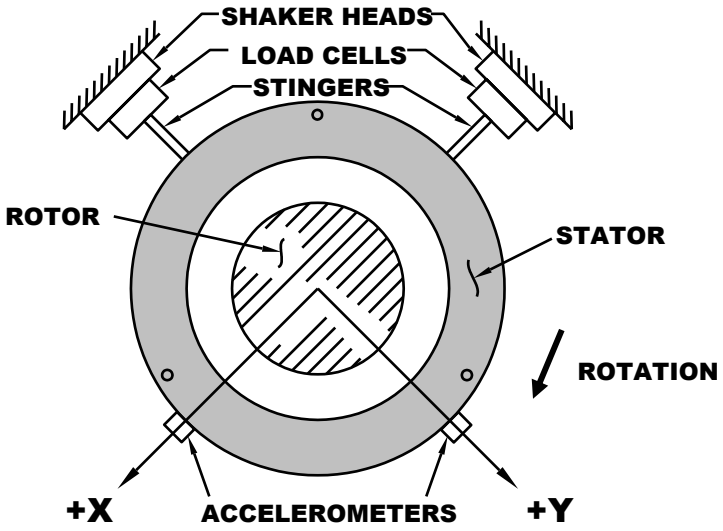

Fig. 4 - Shaker-stinger-stator configuration (view from the non-driven end)

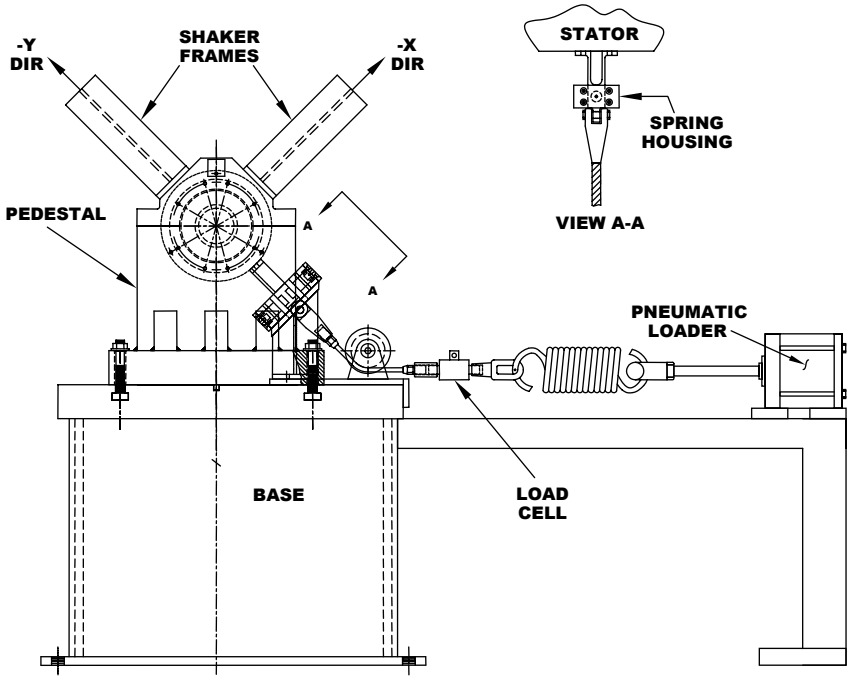

Fig. 5 - Static loader arrangement – (view from non-driven end)

connected to the stator assembly through a pulley and a yoke, and a spring system assures that the load is applied exclusively in one direction. The applied load is measured with a load cell attached to the cable. The rated maximum available load is 22000 N [4945 lbf].

INSTRUMENTATION

Figure 6 shows the stator assembly, which is comprised of the test seals, seal housings and main stator section. The oil is supplied to the seal through two opposing entry ports placed in the main stator section. The oil flows through a circumferential groove in the main stator section and then through the seals. Single tooth labyrinth seals are located at the outlets of the seal housings to keep the oil from exiting freely in the axial direction. This configuration is often referred to as "flooded" lubrication.

Four proximity probes, located in the stator seal housing record the relative motion of the stator with respect to the rotor for each direction of excitation (see Fig 6). Two proximity probes are placed in a plane at the non-driven end and two at a parallel plane at the driven end. Measurement of the stator position in two parallel planes allows monitoring of the stator's pitch and yaw.

Piezoelectric accelerometers measure the stator absolute acceleration in both the x and y directions. Temperature probes are located in the main stator section as well as the seal housings (see Fig 6). A static pressure transducer measures the oil pressure in the inlet channel and a conventional bourdon-type pressure gauge measures the oil outlet pressure, which is close to ambient, i.e., 0.1 bar [~0 psig].

SEAL GEOMETRY

Table 1 summarizes the geometric characteristics and operating conditions of the test seal. Figure 7 shows the seal geometry.

Table 1 - Seal geometry and operating conditions

Radial Seal Clearance - measured	0.085 mm [0.0033 in]
Seal ID - measured	116.98 mm [4.6057 in]
Lubricant	ISO VG 32 Turbine Oil
Target Oil Inlet Temperature	50º C [122º F]
Operating Speeds	4000-10000 rpm
Eccentricity	0.0 - 0.7

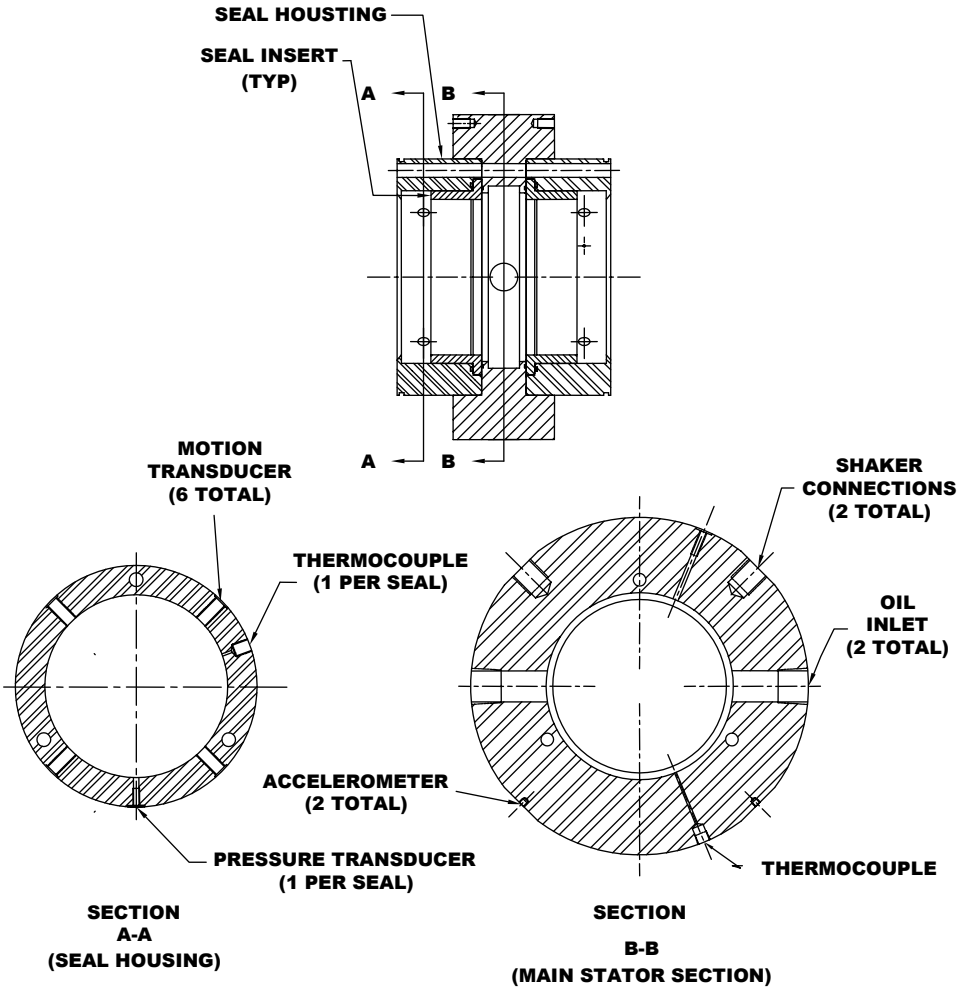

Fig. 6 - Seal stator configuration and instrumentation

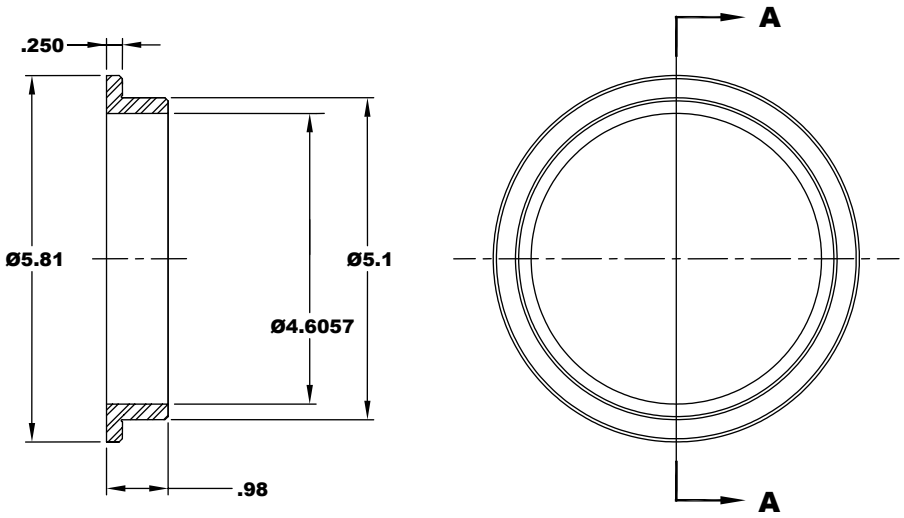

Fig. 7 - Seal geometry

THEORETICAL BACKGROUND[4]

PARAMETER IDENTIFICATION MODEL

This section details the rotordynamic parameter identification procedure and has been adapted from Childs and Hale [15] and Rouvas and Childs [16]. The equations of motion for the stator mass M_s can be written as:

$$M_s \begin{bmatrix} \ddot{x}_s \\ \ddot{y}_s \end{bmatrix} = \begin{bmatrix} f_x \\ f_y \end{bmatrix} - \begin{bmatrix} f_{sx} \\ f_{sy} \end{bmatrix} \tag{1}$$

where $\ddot{x}_s$, $\ddot{y}_s$ are the *measured* components of the stator's acceleration, f_x , f_y are the *measured* excitation force, f_{sx} , f_{sy} are the seal reaction force components. The *x* and *y* subscripts in these equations identify the *x* and *y* direction, as depicted in Fig. 8.

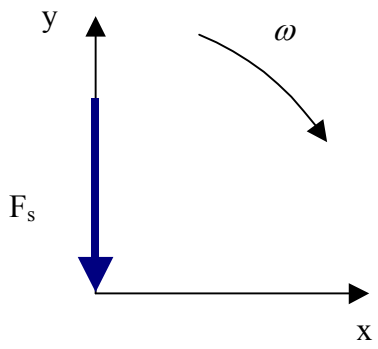

Fig. 8 - Coordinate reference frame

The definition of the seal reaction force as a function of the rotordynamic coefficients is given by:

---

[4] This section, which is a summary of [15] and [16], is adapted with permission from Rodriguez [2].

$$-\begin{bmatrix} f_{sx} \\ f_{sy} \end{bmatrix} = \begin{bmatrix} K_{xx} & K_{xy} \\ K_{yx} & K_{yy} \end{bmatrix}\begin{bmatrix} \Delta x \\ \Delta y \end{bmatrix} + \begin{bmatrix} C_{xx} & C_{xy} \\ C_{yx} & C_{yy} \end{bmatrix}\begin{bmatrix} \Delta \dot{x} \\ \Delta \dot{y} \end{bmatrix} + \begin{bmatrix} M_{xx} & M_{xy} \\ M_{yx} & M_{yy} \end{bmatrix}\begin{bmatrix} \Delta \ddot{x} \\ \Delta \ddot{y} \end{bmatrix} \tag{2}$$

Here $\Delta x, \Delta y$ are defined as the relative motion between the rotor and the stator and K_{ij}, C_{ij}, M_{ij} are matrices elements referring to stiffness, damping and added-mass coefficients, respectively. Substituting Eq. 1 in Eq 2 and rearranging, we obtain:

$$\begin{bmatrix} f_x - M_s \ddot{x}_s \\ f_y - M_s \ddot{y}_s \end{bmatrix} = -\begin{bmatrix} K_{xx} & K_{xy} \\ K_{yx} & K_{yy} \end{bmatrix}\begin{bmatrix} \Delta x \\ \Delta y \end{bmatrix} - \begin{bmatrix} C_{xx} & C_{xy} \\ C_{yx} & C_{yy} \end{bmatrix}\begin{bmatrix} \Delta \dot{x} \\ \Delta \dot{y} \end{bmatrix} - \begin{bmatrix} M_{xx} & M_{xy} \\ M_{yx} & M_{yy} \end{bmatrix}\begin{bmatrix} \Delta \ddot{x} \\ \Delta \ddot{y} \end{bmatrix} \tag{3}$$

The left hand vector of Eq. 3 is a known function of time. On the right hand side, $\Delta x(t)$ and $\Delta y(t)$ are measured functions of time. The rotordynamic coefficients are determined in the frequency domain via the Fast Fourier Transform version of Eq. 3, as shown below.

$$\begin{bmatrix} F_x - M_s A_x \\ F_y - M_s A_y \end{bmatrix} = -\begin{bmatrix} H_{xx} & H_{xy} \\ H_{yx} & H_{yy} \end{bmatrix}\begin{bmatrix} D_x \\ D_y \end{bmatrix} \tag{4}$$

where $F_k = \mathbf{F}(f_k)$, $A_k = \mathbf{F}(\ddot{K}_s)$, and $D_k = \mathbf{F}(\Delta k)$

The elements of the seal dynamic stiffness function ***H*** are related to the coefficients defined in Eq. 3 by:

$$\boldsymbol{H}_{ij} = (K_{ij} - \Omega^2 M_{ij}) + \boldsymbol{J}(\Omega C_{ij}) \tag{5}$$

Where the Real part is $\mathrm{Re}(H_{ij}) = K_{ij} - \Omega^2 M_{ij}$ and the Imaginary part is $\mathrm{Im}(H_{ij}) = \Omega C_{ij}$ and Ω=Excitation frequency and $\boldsymbol{J} = \sqrt{-1}$.

Equation 4 provides only two equations for four unknowns $\boldsymbol{H_{xx}}$, $\boldsymbol{H_{xy}}$, $\boldsymbol{H_{yx}}$, $\boldsymbol{H_{yy}}$. To provide four independent equations, alternate shakes about a given steady-state rotor

position are conducted on the stator in orthogonal directions (*x* and *y*) yielding four equations and four unknowns, given by:

$$\begin{bmatrix} F_{xx} - M_s A_{xx} & F_{xy} - M_s A_{xy} \\ F_{yx} - M_s A_{yx} & F_{yy} - M_s A_{yy} \end{bmatrix} = -\begin{bmatrix} \boldsymbol{H}_{xx} & \boldsymbol{H}_{xy} \\ \boldsymbol{H}_{yx} & \boldsymbol{H}_{yy} \end{bmatrix} \begin{bmatrix} D_{xx} & D_{xy} \\ D_{yx} & D_{yy} \end{bmatrix} \tag{6}$$

One set of frequency-dependent dynamic stiffness coefficients *(**H**xx, **H**xy, **H**yx, **H**yy*) is obtained as the average of 32 separate shake tests, which are averaged in the frequency domain. To estimate the variability of dynamic data, 10 consecutive tests are conducted. During these tests, the operating conditions are held approximately constant ($\Delta P = \pm$ 10 psi, $\Delta\Omega = \pm$100 RPM). The dynamic stiffness data are reduced and the standard deviation of the dynamic stiffnesses and rotordynamic coefficients are obtained for discrete frequencies starting at 20 *Hz* and up to 210 *Hz* with increments of 10 Hz. The standard deviations obtained from these 10 sequential tests define the uncertainty at each frequency for both the baseline and seal tests (see section "Measurement of 'Baseline' Dynamic Stiffness" on pg 19 for explanation of baseline tests).

Uncertainties in the dynamic stiffness coefficient results vary with frequency. For example, results near the electrical power frequency of 60 Hz or multiples of this frequency are consistently poor, and the reduced data at these frequencies are ignored. The test uncertainty is calculated at each frequency as the square root of the sum of the squares of the baseline uncertainty (negligible in this case) and seal test uncertainty at each frequency.

CURVE-FITTING PROCEDURE AND UNCERTAINTY ANALYSIS

The procedure used for acquiring the estimates for the seal stiffness, damping and added mass coefficients by using linear regression is detailed in Rodriguez [2]. The seal stiffness coefficients (Kxx, Kxy, Kyx, Kyy) are estimated from the regression line intercepts of the real parts while the regression line slope of the real parts estimates the seal added mass coefficients (Mxx, Myy). The seal damping coefficients (Cxx, Cxy,

Cyx, Cyy) are estimated from the regression line slope of the imaginary parts. In the case of the imaginary parts, the intercept is ignored because it has no physical meaning. “Estimates” is used because the coefficients are calculated rather than measured directly and that only a finite amount of data is taken. Rodriguez [2] also details the uncertainly analysis used in the data reduction.

EXPERIMENTAL PROCEDURE

During a typical test, the shaft is brought up to steady state conditions for running speed (± 100 RPM) eccentricity, differential pressure (± 10 psi) and oil inlet temperature (± 5 ºC). Dynamic data, oil leakage rate and the other steady state condition listed above are taken at the conditions shown in Table 2.

Table 2 - Test conditions[5]

Pressure / ω		[bar]		
		21	*45*	*69*
[RPM]	*4000*	✓	✓	✓
	7000	✓	✓	✓
	10000	✓	✓	✓

The target inlet oil temperature for all tests was 50º C [122º F]. The seal housing is then alternately excited using the hydraulic shakers with a pre-specified pseudo-random dynamic excitation in two orthogonal directions, i.e. *x*-direction and the *y*-direction (static load direction). Dynamic data include the seal relative motion with respect to the shaft at the driven and the non-driven end, forces applied by the shakers and absolute acceleration of the seal stator. The data are captured in the time domain and later transformed to the frequency domain with the Fast Fourier Transform and reduced with the procedure described earlier.

[5] All tests were performed at nominal eccentricities of 0, 0.3, 0.5, 0.6, and 0.7; however, some of the higher eccentricities could not be obtained for every test case due to excess test oil or support bearing temperatures or for fear of the seal contacting the rotor.

MEASUREMENT OF 'BASELINE' DYNAMIC STIFFNESS

These tests aim to measure rotordynamic coefficients of the test seal. However, the measurement procedure also measures stiffness, damping and inertia introduced by anything that is attached to the seal – i.e. the pitch stabilizers, hose connections, etc (refer to Fig. 3). To account for these additional elements, 'base-line' tests were conducted with 'dry shakes' at zero rotor speed and no oil supplied to the seals. Figures 9 through 11 show the direct and cross-coupled, real and imaginary, baseline dynamic stiffness coefficients vs frequency. These baseline dynamic stiffnesses will be subtracted from the values obtained for the test dynamic stiffnesses to determine the dynamics caused only by the seal.

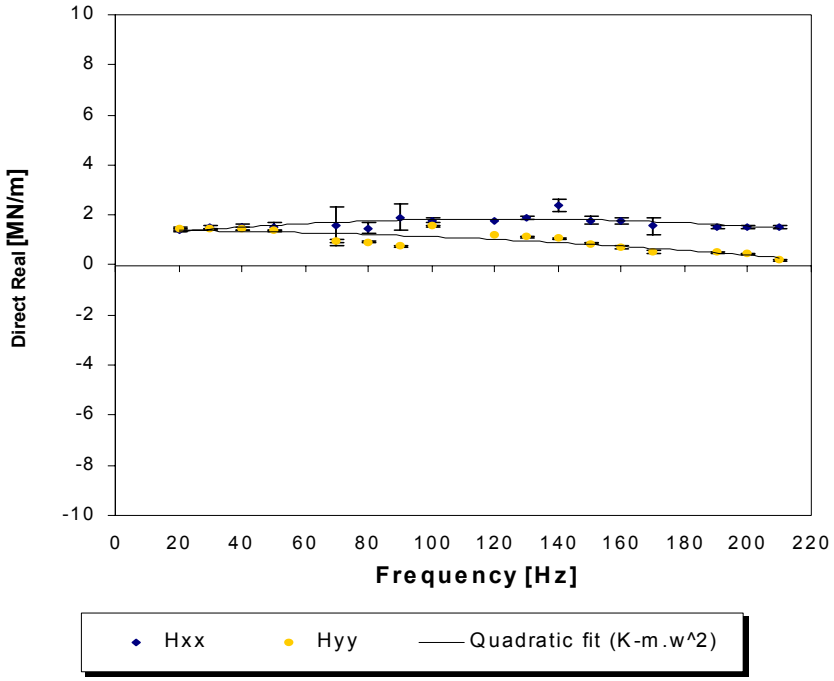

Fig. 9 - Baseline real direct dynamic stiffness

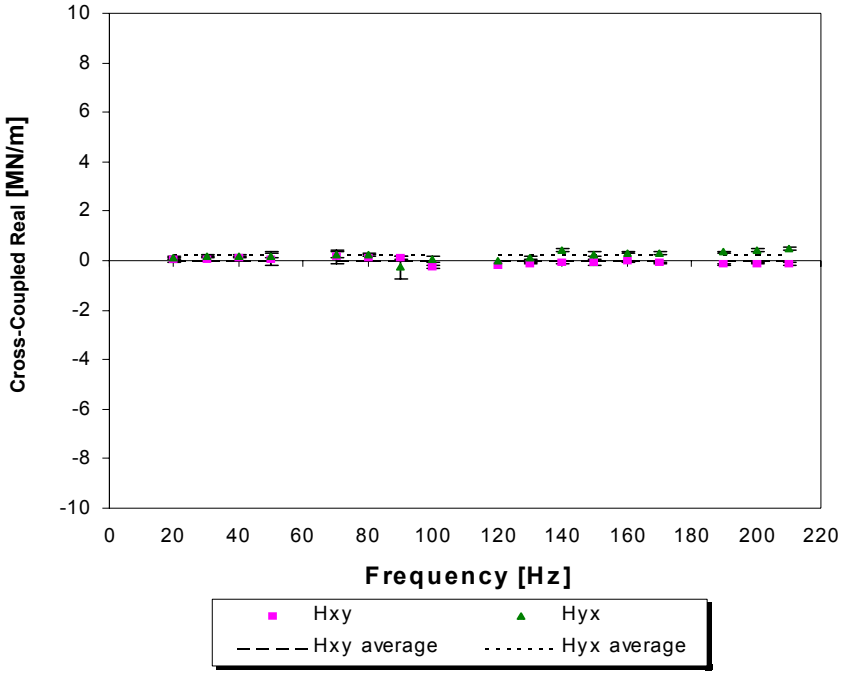

Fig. 10 - Baseline real cross-coupled dynamic stiffness

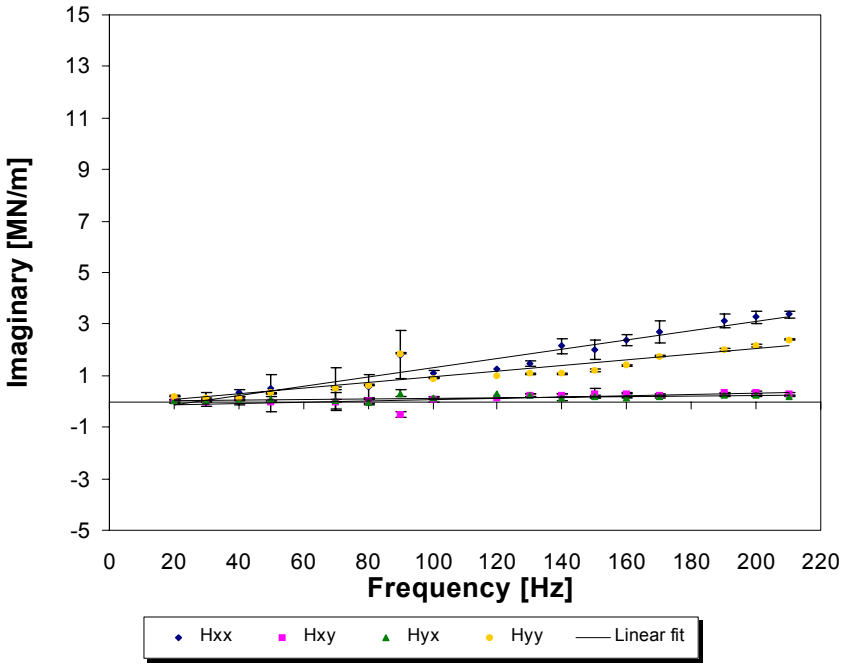

Fig. 11 - Baseline imaginary dynamic stiffness

STATIC PERFORMANCE CHARACTERISTICS[6]

SEAL LEAKAGE

The oil flow rates predicted via XLLubeGT and the actual oil flow rates as a function of eccentricity can be seen in Fig. 12. The results from XLAnSeal are not shown because they are essentially identical. The dominant factor for the oil flow rate is the differential pressure across the seal and not the running speed. Greater eccentricities will, however, also cause more leakage. The results in Fig 12 follow the expected trends and correlate reasonably well with the theoretical values, but the theory does have a tendency to under-predict the leakage for all eccentricities and the seal load at higher eccentricities.

ROTOR CENTER LINE LOCI

Figure 13 shows the average rotor center-line loci for the experimental data as a function of attitude angle and eccentricity. These figures represent the loci of the rotor as viewed from the non-driven side of the test apparatus. There is no rotor center-line loci based on the theoretical data, because the eccentricities in Fig. 13 were used as input parameters to XLLubeGT and XLAnSeal and hence would give the same plots. 0º corresponds to the positive X direction and 270º corresponds to the positive Y direction. As expected, the rotor moves from the centered position to the negative X direction as the eccentricity increases. As the eccentricity continues to increase, the rotor begins to move in the direction of the static load or positive Y direction. [17]

---

[6] On the results plots, the data labels prefixed with a "t_" (e.g. t_Load) are the values produced from XLLubeGT and/or XLAnSeal ("theoretical"), while the data labels without a "t_" prefix are the values acquired from the test rig ("experimental").

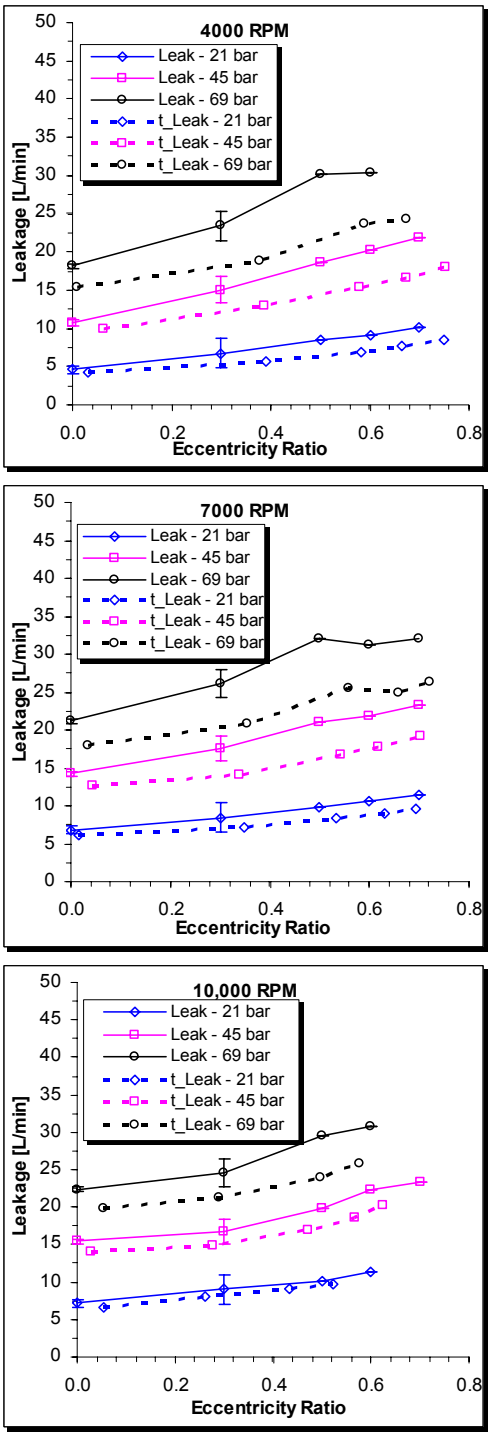

Fig. 12 - Seal leakage: experimental vs theory (XLLubeGT)

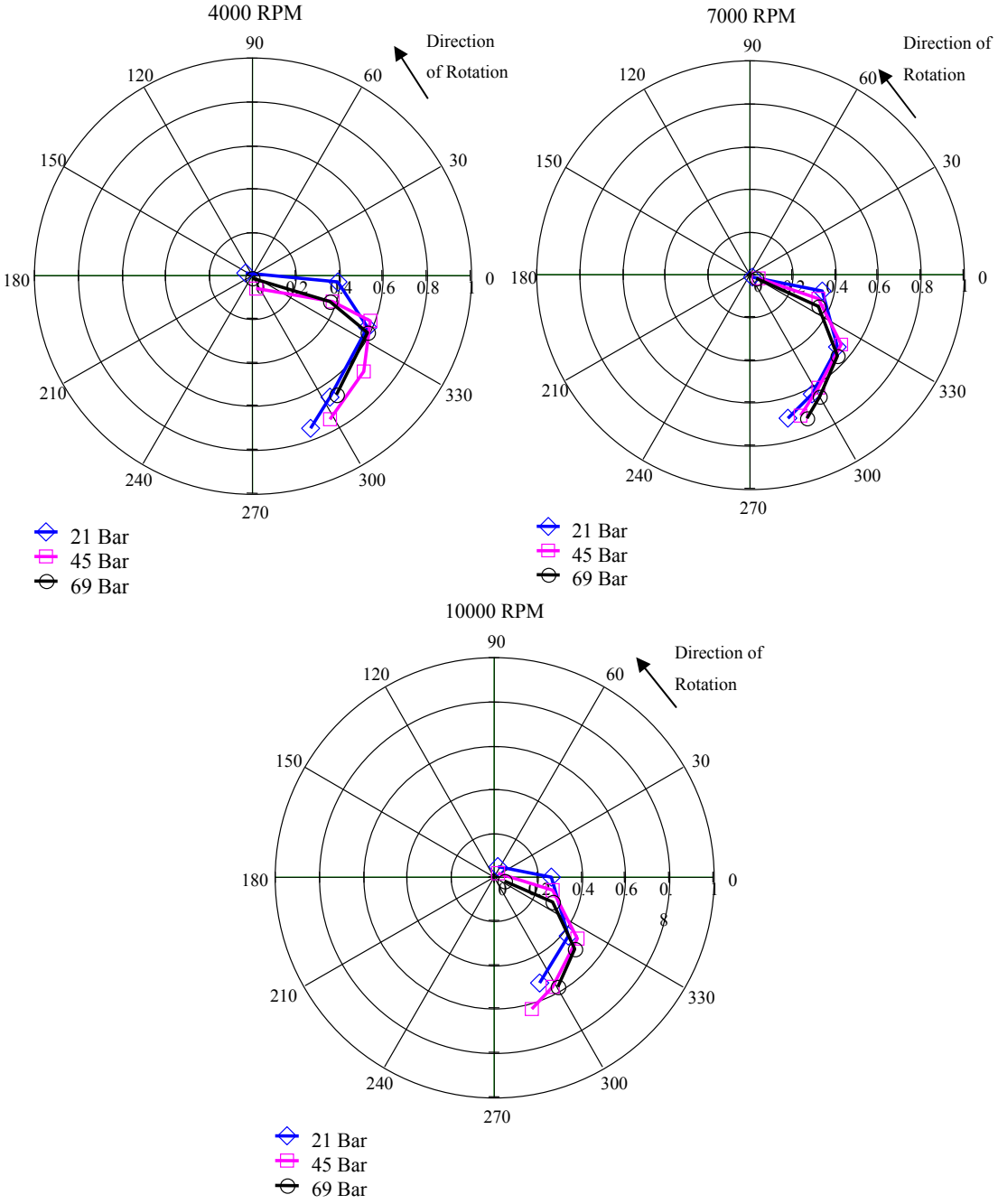

Fig. 13 - Average rotor center line loci for static operating points

REYNOLDS NUMBERS

To show that the flow regimes within the seal are strongly laminar (Re < 2000), the Circumferential, Axial and Squeeze Reynolds numbers (Eq. 8, 9 and 10, respectively) were calculated using experimental data from a high-pressure, high-speed test. The conditions listed in Table 3 were used to calculate the Reynolds numbers:

Table 3 - Test conditions for Reynolds calculations

$\omega = 10{,}000 \cdot RPM$	Running speed
$\Delta p = 68.9 \cdot bars$	Differential pressure across the seal
$e = 0.3$	Seal nominal eccentricity
$T_{avg} = 59.7 \cdot ^{o} C$	Average temperature of the oil inlet and outlet temperature

$$\mathrm{Re}_{CIRC} = \frac{\rho \cdot \omega \cdot r \cdot Cr}{\mu} = 308.9 \tag{8}$$

$$\mathrm{Re}_{AXIAL} = \rho \frac{\dot{Q}}{2\pi r \mu} = 66.1 \tag{9}$$

$$\mathrm{Re}_{SQUEEZE} = \frac{\rho \cdot \omega \cdot Cr^{2}}{\mu} = 0.45 \tag{10}$$

DYNAMIC STIFFNESS AND ROTORDYNAMIC COEFFICIENTS

SEAL DYNAMIC STIFFNESS

Figures 14, 15 and 16 show an example set of results for the real and imaginary dynamic stiffness acquired from the test rig with the test conditions of RPM = 4000, ΔP = 44.8 bar [649.7 psi] and e = 0.3. These plots have the baseline stiffness (Fig. 9 - 11) subtracted out. As discussed in the section "Curve-fitting Procedure and Uncertainty Analysis" (pg 15), the slopes of the real dynamic stiffness data (**H**xx, **H**yy, **H**xy, **H**yx) defines Mxx, Myy, Mxy and Myy, respectively; while the intercepts define Kxx, Kyy, Kyx and Kyx, respectively. The slopes of the imaginary parts of the dynamic stiffness define Cxx, Cyy, Cxy, Cyx, respectively. As stated previously, the intercepts of the imaginary parts has no physical meaning and is therefore ignored.

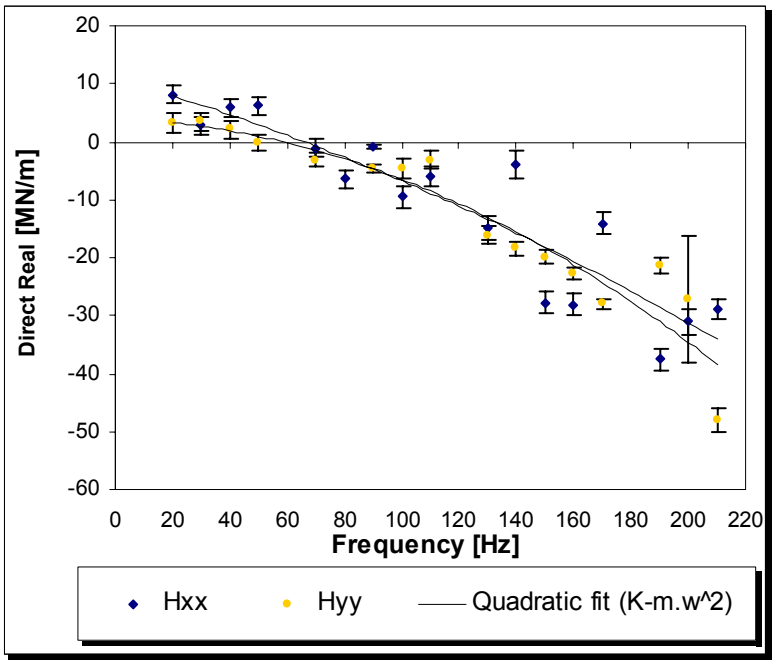

Fig. 14 - Real direct dynamic stiffness

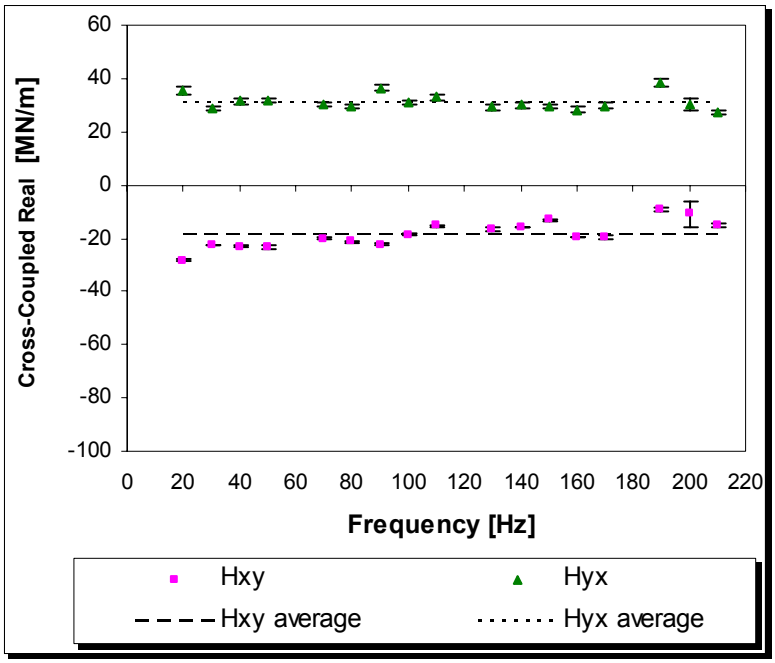

Fig. 15 - Real cross-coupled dynamic stiffness

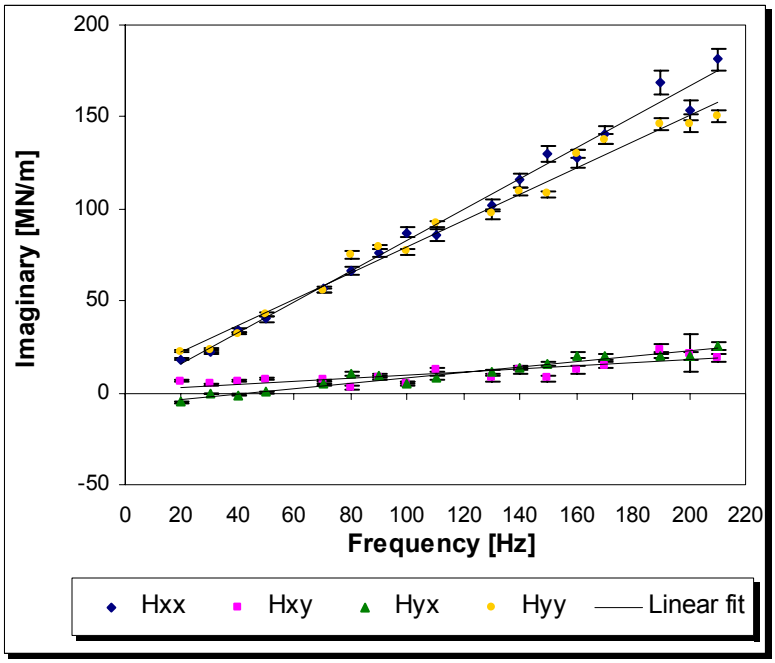

Fig. 16 - Imaginary direct and cross-coupled dynamic stiffness

ROTORDYNAMIC COEFFICIENTS[7]

In this section, the experimental and theoretical results are shown in the following figures: direct and cross-coupled stiffnesses are shown in Figs. 17 and 18; direct and cross-coupled damping are shown in Figs. 19 and 20; direct inertial coefficients are shown in Fig. 21. The data in Figs. 17 thru 21 were obtained by using the previously described parameter identification model. The data are shown as a function of eccentricity and running speed with uncertainty bars included for each data point. The results from XLAnSeal, except for the direct inertial terms, are not shown because they are essentially the same as those reported by XLLubeGT. The plots for the added mass as calculated by XLLubeGT were not shown because XLLubeGT predicts these terms to be zero or negligible.

The assumption for the data interpretation, theoretical and experimental, is that it would look similar to Ocvirk's short bearing solution. When initially looking at the theoretical rotordynamic coefficients, the cross-coupled stiffness and damping terms did not follow these trends. On closer inspection, it was determined that a conversion was needed to properly compare the experimental and theoretical results. This was due to the difference in the assumed coordinate systems and directions of rotation of the test rig and the code. The conversion was determined by using vector algebra and resulted in the realization that both the cross-coupled stiffness and damping terms from the code results needed to be multiplied by (-1).

In order to make the experimental data follow the short bearing solution, all cross-coupled results except the Kyx term were also to be multiplied by (-1). This is logical because the short bearing solution assumes that the Cxy and Cyx terms are equal and negative while the Kxy and Kyx terms are equal and opposite. Even with these two conversions, there were two final discrepancies that had to be dealt with. The

---

[7] On the results plots, the data labels prefixed with a "t_" (e.g. t_Cxx) are the values produced from XLLubeGT and/or XLAnSeal ("theoretical"), while the data labels without a "t_" prefix are the values acquired from the test rig ("experimental").

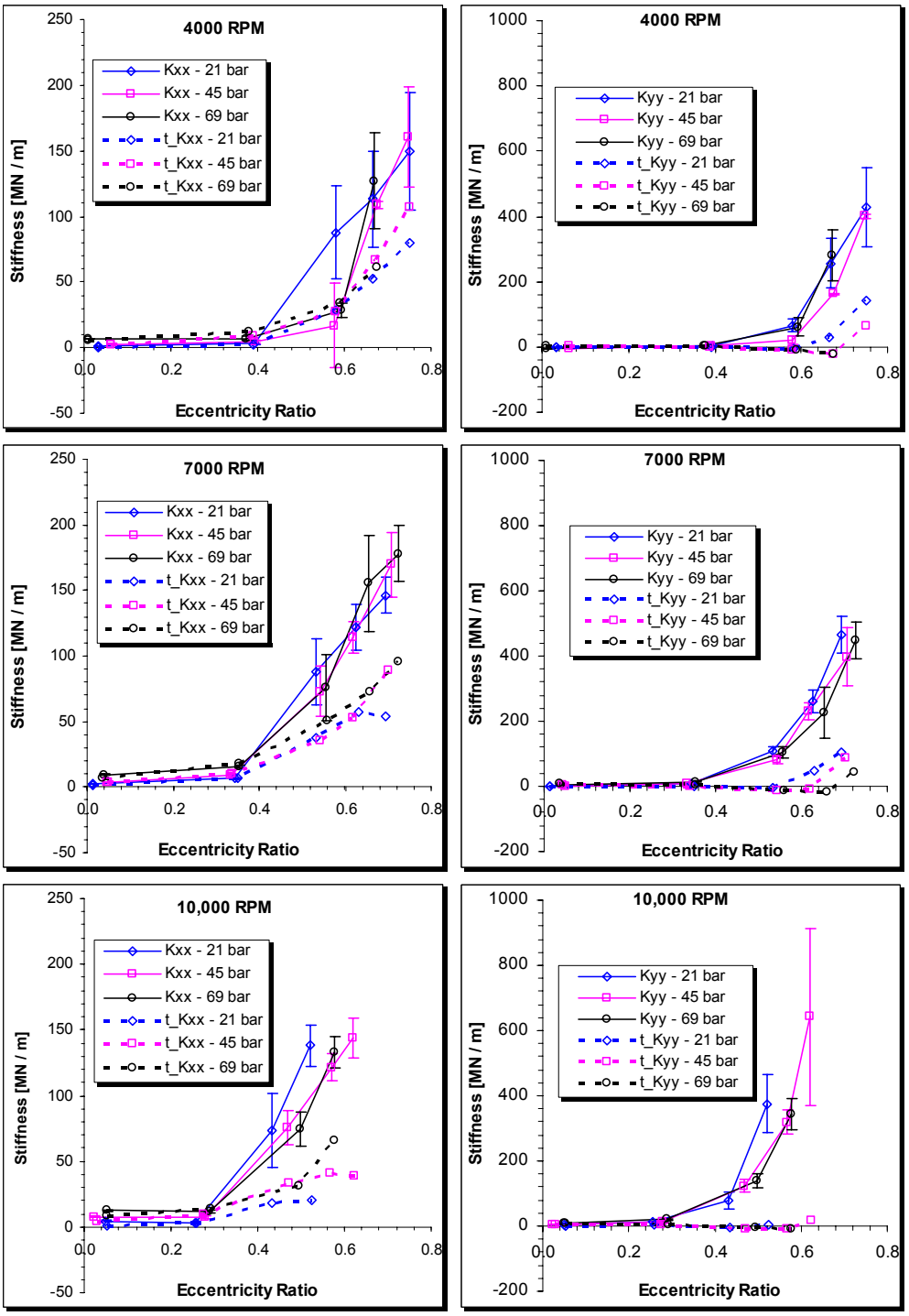

Fig. 17 - Seal direct stiffness coefficients exp. vs theory (XLLubeGT)

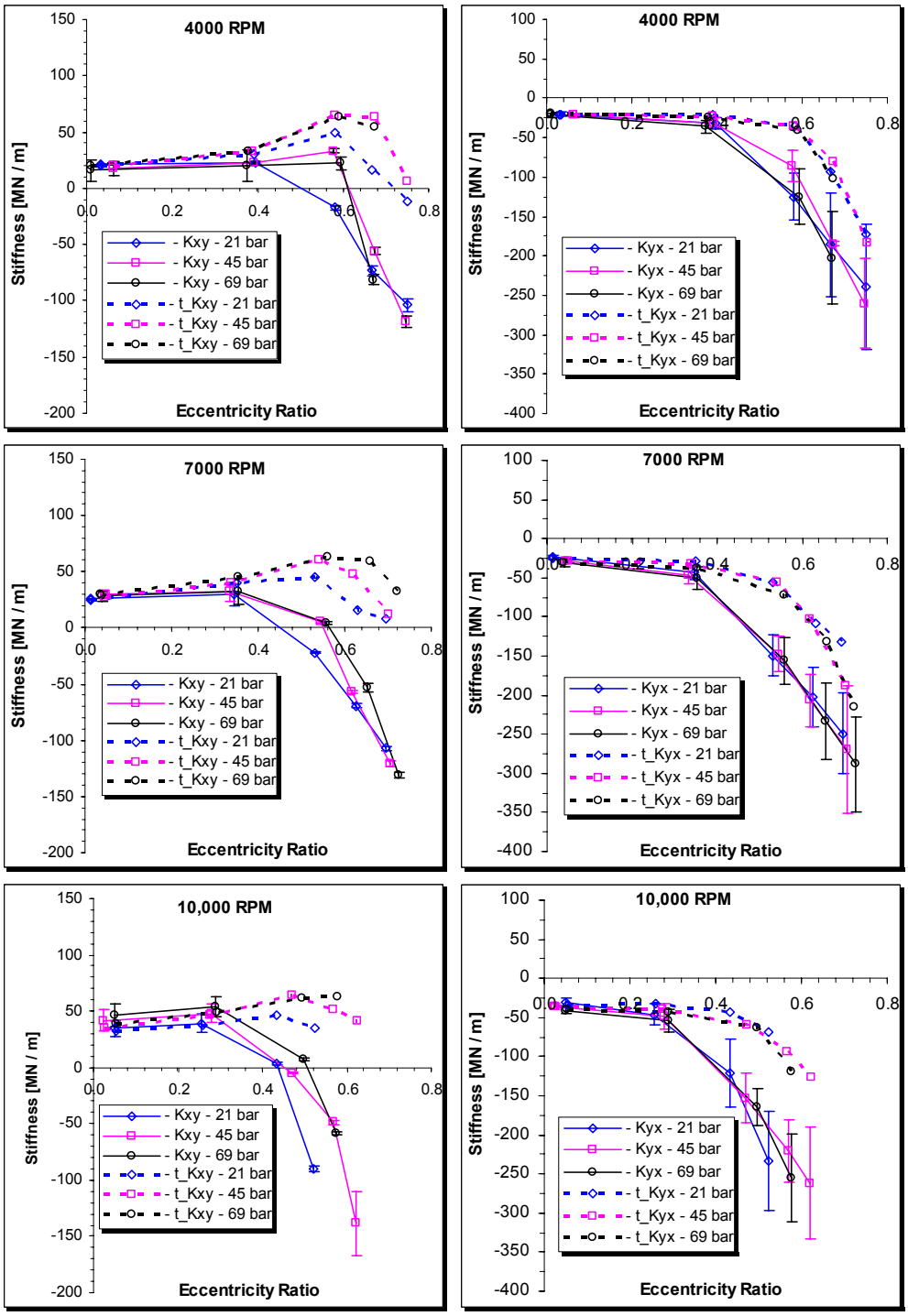

Fig. 18 - Seal cross-coupled stiffness coefficients exp. vs theory (XLLubeGT)

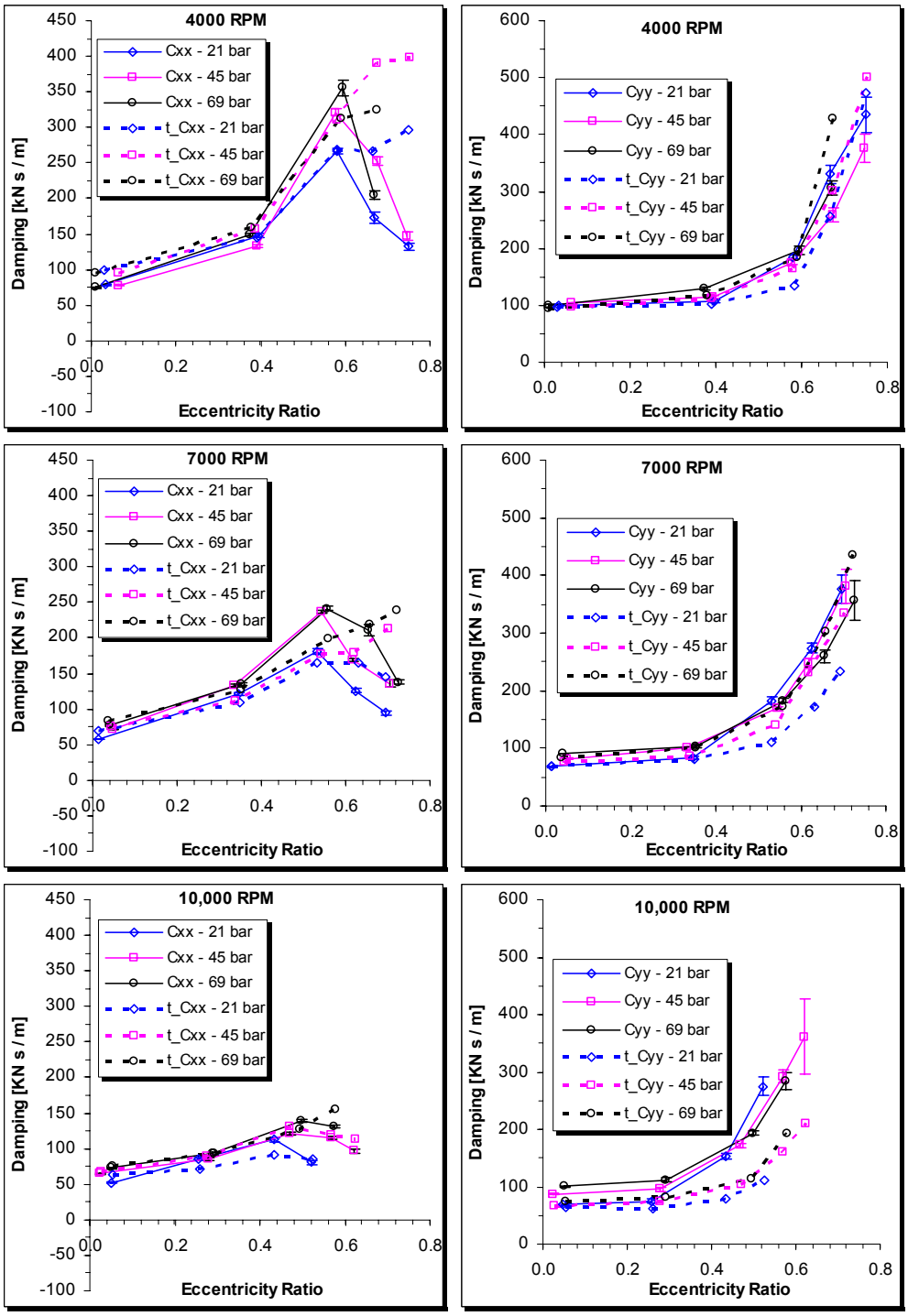

Fig. 19 - Seal direct damping coefficients exp. vs theory (XLLubeGT)

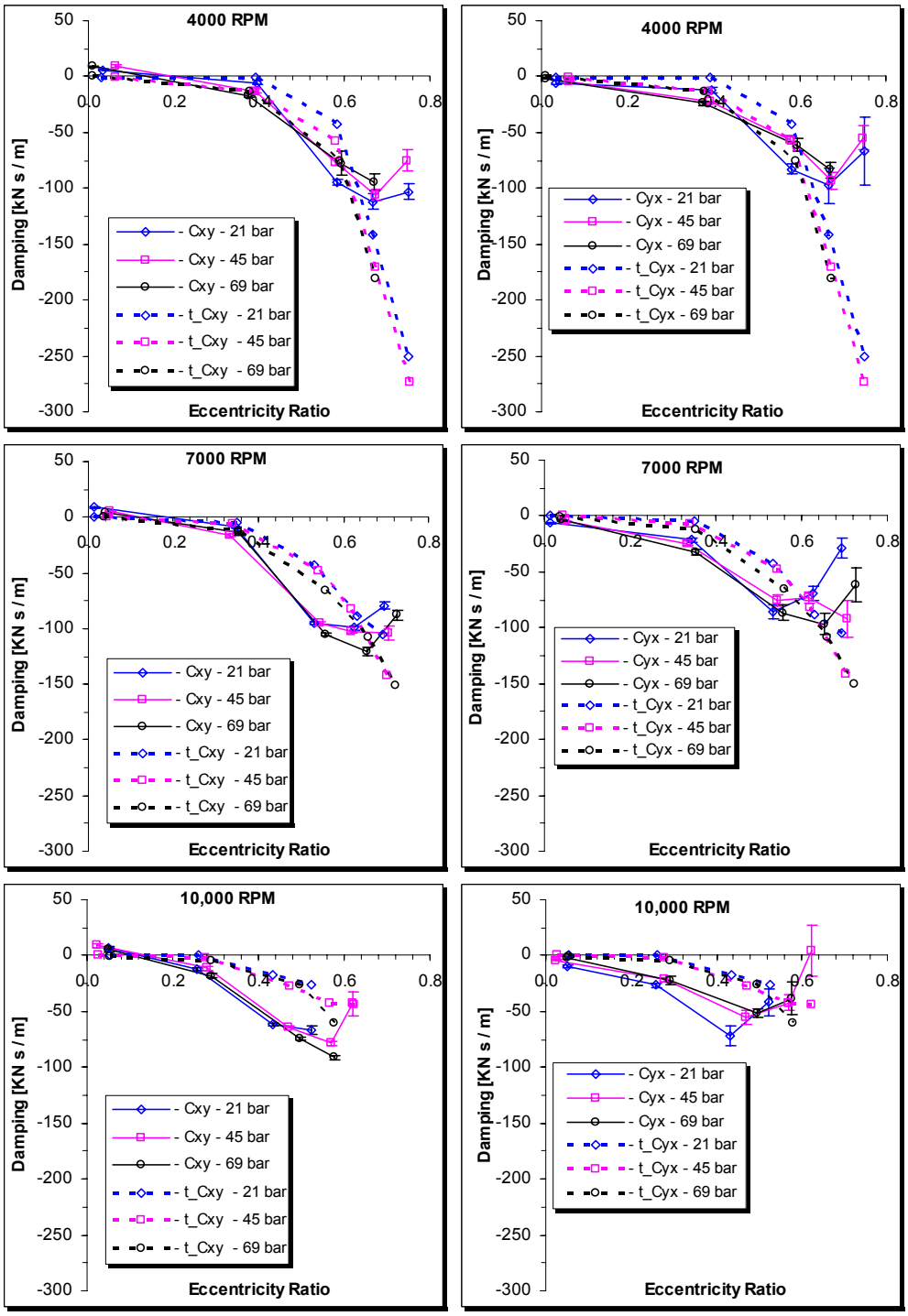

Fig. 20 - Seal cross-coupled damping coefficients exp. vs theory (XLLubeGT)

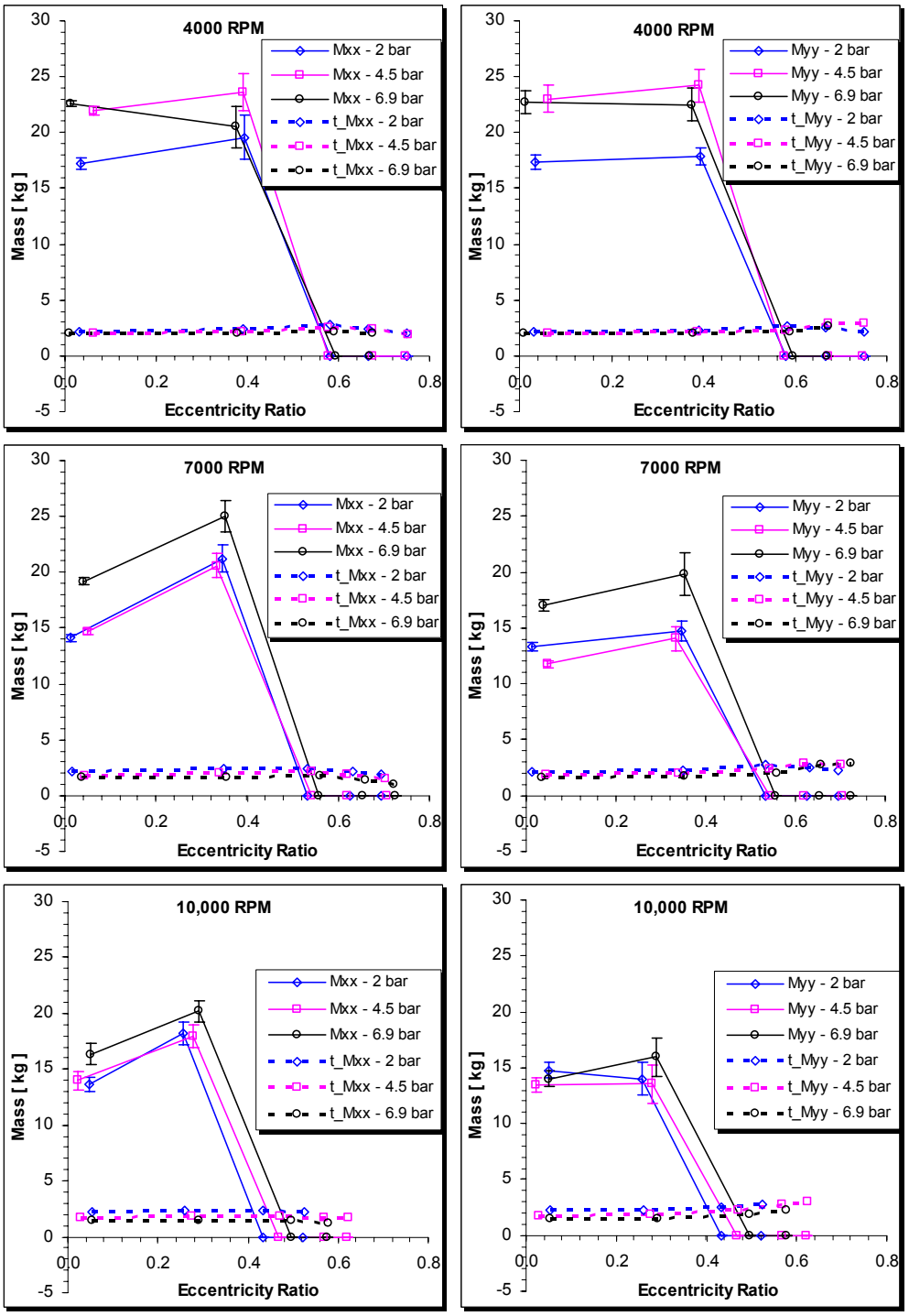

Fig. 21 - Seal added-mass coefficients - exp vs theory (XLAnSeal)

discrepancies were with the theoretical Kxy and Kyx values. They still did not follow the short bearing solution. In order to make them fit, the Kxy and Kyx values were interchanged. The author made detailed examinations into the data reduction and determined that there were no errors causing the values to be switched. The only probable sources of error remaining are an output error in the code, code implementation or the different coordinate system conventions.

After doing these conversions, the experimental and theoretical data followed the trends predicted by Ocvirk's solution and correlated well with each other. At lower eccentricities, the experimental and theoretical values for each coefficient are almost the same regardless of differential pressure. There was a point were the two sets of values began to diverge from each other, and this point decreased as the running speed increased. All of the stiffness coefficients diverged at approximately the same eccentricities which were 0.4, 0.35 and 0.3 for 4000, 7000 and 10,000 RPM, respectively. The direct damping values tended to diverge at higher eccentricities; for Cxx the values were 0.6, 0.55, and 0.5 for 4000, 7000 and 10,000 RPM, respectively. At the divergence of the Cxx values, the experimental data "turned down" with a negative slope while the theory continued upwards with a positive slope. The Cyy values tended to diverge only until higher running speeds and this point was at an eccentricity of about 0.3. Divergence for the cross-coupled damping values was at approximately 0.6, 0.35, 0.3 for 4000, 7000 and 10,000 RPM, respectively. At the divergence, the experimental data "turned up" with a positive slope while the theory continued with a negative slope.

The experimentally determined inertial terms follow the expected trends: non-negligible at centered and lower eccentricities and zero or negligible at higher eccentricities. The inertial terms are assumed to be negligible at higher eccentricities because the fluid shear forces are dominant. This is due to the reduced flow area between the rotor and seal which causes increased flow velocities. Bulk flow predictions of XLAnSeal show the inertial terms are greatly under-predicted and that the inertial terms are always present for all eccentricities. As mentioned previously, there are no theoretical direct mass terms given from XLLubeGT.

WHIRL-FREQUENCY RATIO[8]

The Whirl-Frequency Ratio (WFR) is the ratio of the frequency of rotor precession to the frequency that the rotor-seal system becomes unstable (Onset speed of instability). Therefore the WFR can be used to determine the stability of a rotor-seal system. The closer the ratio is to 1 the more unstable the system is, and the opposite is true as the ratio approaches zero. Generally for seals, the WFR is equal to about 0.5. Figure 22 provides the experimental and theoretical whirl-frequency ratio as a function of eccentricity and of running speed. The WFR was calculated by using the following equations:

$$Keq = \frac{Kxx * Cyy + Cxx * Kyy - Cyx * Kxy - Cxy * Kyx}{Cxx + Cyy} \tag{11}$$

$$WFR = \sqrt{\frac{(Keq - Kxx) * (Keq - Kyy) - (Kxy * Kyx)}{\omega^2 (Cxx * Cyy - Cxy * Cyx)}} \tag{12}$$

The theoretical and experimental values compare well at lower eccentricities, but differ greatly at higher eccentricities. The results do show similarities to those for a plain journal bearing in that the WFR goes to zero at higher eccentricities. However, the point at which the WFR turns down and goes toward zero tends to be higher than what the experimental data is showing. The data also shows that as the running speed increases, the rotor becomes more stable. This can also be seen in the results for the rotor center line loci (Figure 13). As the eccentricity is increased at higher running speeds, the path the rotor takes is more "flat" as compared to the path the rotor takes at lower speeds. This "flatness" can be attributed to reduced magnitudes of the cross-coupled terms. It is these cross-coupled terms that tend to create a deflection in one

[8] On the results plots, the data labels prefixed with a "t_" (e.g. t_Cxx) are the values produced from XLLubeGT and/or XLAnSeal ("theoretical"), while the data labels without a "t_" prefix are the values acquired from the test rig ("experimental").

coordinate direction from a force in another coordinate direction. Note that the static loader applies a load in the +y or 270º direction and if there were no cross-coupled terms, the rotor center line loci would be a straight line in the +y direction.

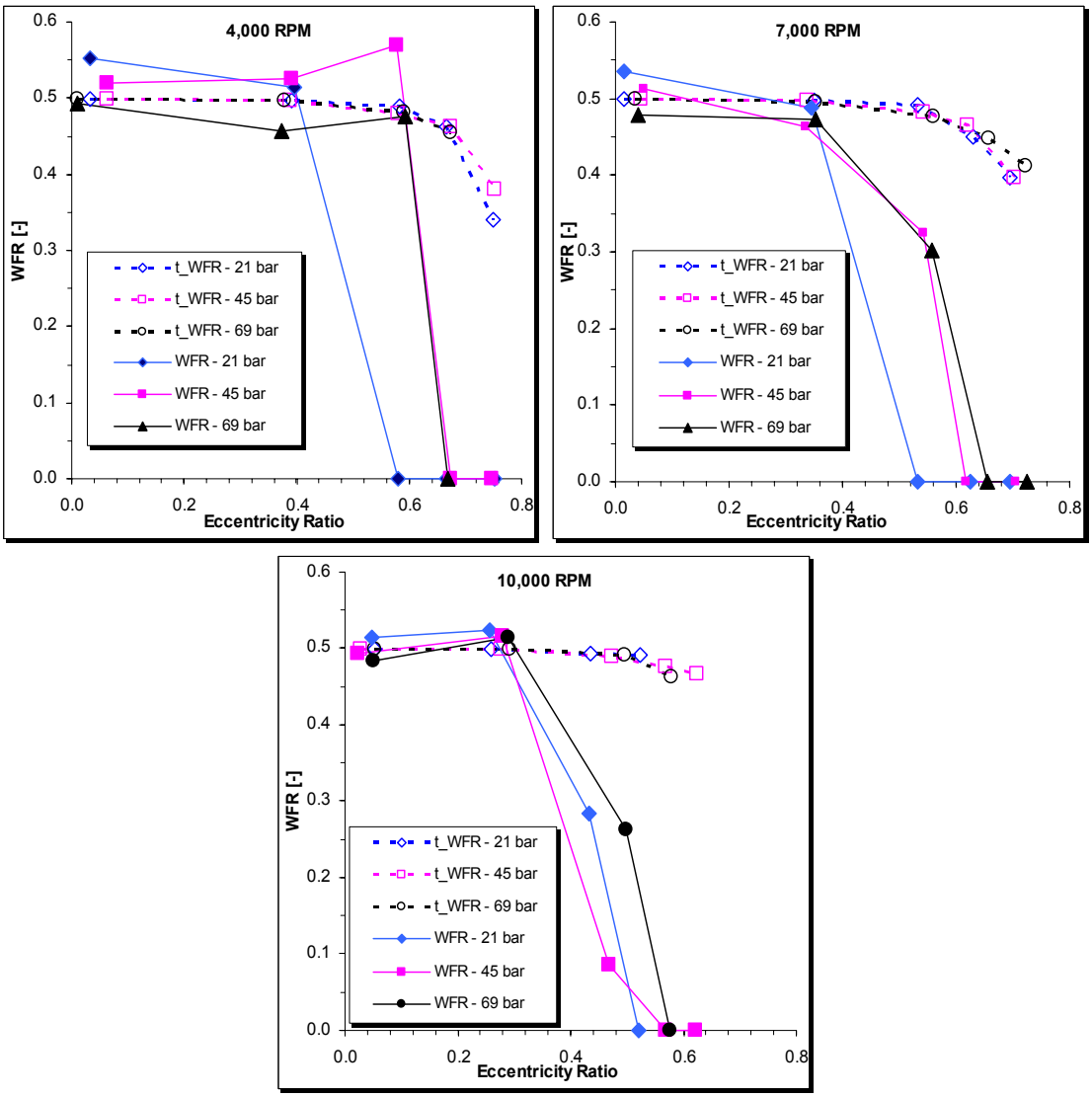

Fig. 22 - Whirl frequency ratio - experimental vs theory (XLLubeGT)

CONCLUSIONS AND RECOMMENDATIONS

CONCLUSIONS

This thesis provides a comparison of experimental rotordynamic coefficients for laminar, smooth, bushing oil seals to that of theoretical predictions from XLLubeGT and XLAnSeal. The experimental data was collected from a new test rig at the Turbomachinery Laboratory at Texas A&M University. XLLubeGT and XLAnSeal are computer programs used to predict the rotordynamic coefficients and leakage characteristics of seals. XLLubeGT uses a Reynolds Equation based solution while XLAnSeal uses a bulk-flow Navier Stokes solution which includes temporal and convective fluid accelerations. The input values for the seal codes were the actual measured test conditions from the test rig. Fluid inlet inertia effects and thermal gradients along the seal were included in the input parameters. The dynamic characteristics that were reported include stiffness, damping, inertia terms and WFR. Test conditions include three shaft speeds (4000, 7000 and 10,000 rpm), three test pressures (21, 45 and 69 bar [300, 650 and 1000 psi] and multiple eccentricities from 0.0 to 0.7. Seal static characteristics are also reported. They include: leakage and rotor center-line loci.

Dynamic performance results show that all terms are strongly eccentricity dependent with a lesser dependency on running speed and differential pressure. The theoretical predictions from XLLubeGT and XLAnSeal (except the Mxx and Myy terms) tended to agree with the experimental data up to an eccentricity of about 0.5 despite the added mass terms being so large. The seal leakage trends are predicted well; however, the actual leakage is generally under-predicted. The discrepancy between theory and experiment leakage increases with greater Δp. The WFR and rotor center line loci results show that as the running speed increases, the rotor becomes more stable due to reduced amounts of cross-coupled characteristics. Also the system stability (WFR) is under-predicted by the seal codes at higher eccentricities. The experimental data also

shows significant added mass terms up to eccentricities of about 0.35. Usually, the effect of the fluid inertia is neglected when calculating the dynamic coefficients of oil seals on the basis that the flow regime is mostly laminar. However, the results of this paper show that there are significant added mass terms which can be predicted by a bulk flow model. XLAnSeal was used to predict the added mass terms, but it greatly under-predicted these values.

The differences in the theory and experimental results could be due in part to neglecting the seal deformation. As mentioned previously, Venkatarman and Palazzolo [8], Bahetti and Kirk [9] show that if the differential pressure is high enough, the seal will deform and create a converging taper. Bahetti and Kirk also found that neglecting the deformations tended to under-predict the direct stiffness and damping as well as the cross-coupled stiffness. Examining the data, these trends are apparent. Further investigations would need to be done to determine if this is the actual reason, but was not in the scope of this work.

RECOMMENDATIONS

- Include seal bore growth in seal calculations

REFERENCES

[1] Kirk, R.G. and Miller, W., 1979, "The Influence of High Pressure Oil Seals on Turbo-Rotor Stability," ASLE Transactions, **22**, 1, pp 14-27.

[2] Rodriguez, L. E., 2004, "Experimental Frequency-Dependent Rotordynamic Coefficients for a Load-On-Pad, High-Speed, Flexible-Pivot Tilting-Pad Bearing," Master's Thesis, Texas A&M University, College Station, TX.

[3] Semante, J.E. and San Andres, L., 1993, "Analysis of Multi-land High Pressure Oil Seals," Tibology Transactions, **36**, 4, pp. 661-669.

[4] Black, H.F. and Jenssen, D.N., 1971, "Effect of High Pressure Ring Seals on Pump Rotor Vibrations," ASME Paper 71-WA/FE-38.

[5] Black, H.F. and Cochrane, E.A., 1973, "Leakage and Hybrid Bearing Properties of Serrated Seals in Centrifugal Pumps," *6th International Conference on Fluid Sealing*, Munich, Germany, March 1973.

[6] Kirk, R.G. and Nicholas, J., 1980, "Analysis of High Pressure Oil Seals for Optimum Turbo-compressor Dynamic Performance," *Vibrations in Rotating Machinery, Second International Conference*, Institution of Mechanical Engineering, Cambridge, England, September, pp. 125-134.

[7] Reedy, S.W. and Kirk, R.G., 1990, "Analysis of Thermal Gradient Effects in Oil Ring Seals," STLE Tribology Transactions, **33**, 3, pp. 425-435.

[8] Venkataraman, B. and Palazzolo, A. B., 1996, "Effects of Wall Flexibility on the Rotordynamic Coefficients of Turbulent Cryogenic Annular Seals," Journal of Tribology, **118**, pp. 509-519.

[9] Baheti, S.K. and Kirk, R.G., 1999, "Analysis of High Pressure Seal Ring Distortion and Stability Using Finite Element Methods," Journal of Tribology, **121**, pp. 921-925.

[10] Tanaka, M., 1984, "Effect of the Fluid Film Seals on the Stability of Turbo-compressor Rotor." *Proceedings of IFToMM International Conference on Rotordynamics,* Tokyo, Japan.

[11] Kirk, R.G., McKenna, J. and Kraft, D. W., 1986, "Transient Response of Floating Ring Seals: Current Analysis and Future Test Program Requirements," *Post IFToMM Conference on Flow Induced Forces in Rotating Machinery*, Kobe University, Rokko, Nada, Kobe, Japan, Sept 18-19.

[12] Kirk, R.G. and Browne, D.B., 1990, "Experimental Evaluation of Holding Forces in Floating Ring Seals," *Proceedings of the 3rd International Conference on Rotordynamics*, Lyons, France. pp. 319-323.

[13] Kaneko, S., 1984, "Static and Dynamic Characteristics of Annular Plain Seals," *Third International Conference on Vibration in Machinery*. C278. pp 205-214.

[14] Kaul, A., 1999, "Design and Development of a Test Setup for the Experimental Determination of the Rotordynamic and Leakage Characteristics of Annular Bushing Oil Seals," M.S. Thesis, Texas A&M University, College Station, TX.

[15] Childs, D., and Hale, K., 1994, "A Test Apparatus and Facility to Identify the Rotordynamic Coefficients of High-Speed Hydrostatic Bearings," ASME Journal of Tribology, **116**, pp. 337-344.

[16] Rouvas, C., and Childs, D., 1993, "A Parameter Identification Method for the Rotordynamic Coefficients of a High Reynolds Number Hydrostatic Bearing," ASME J. of Vibration and Acoustics, **115**, pp. 264-270.

[17] Vance, J. M., *Rotordynamics of Turbomachinery*, John Wiley and Sons, New York, 1988. pg 215.

VITA

Vittorio Giuseppe Culotta was born in Louisiana. He attended Louisiana Tech University in Ruston, Louisiana, where he received a B.S. in mechanical engineering in 1998. He attended graduate school at Texas A&M University where he fulfilled the requirements for a Master of Science degree in mechanical engineering. He currently works for Mustang Engineering – an engineering firm which provides design and project management services to the oil and gas industry across many sectors.

21623 Canyon Terrace Lane
Katy, Texas 77450